

3D-printable portable open-source platform for low-cost lens-less holographic cellular imaging

Stephan Amann¹, Max von Witzleben¹, Stefan Breuer¹

¹Institute for Applied Physics, Technische Universität Darmstadt, Schlossgartenstraße 7, 64289 Darmstadt, Germany

Digital holographic microscopy is an emerging potentially low-cost alternative to conventional light microscopy for micro-object imaging on earth, underwater and in space. Immediate access to micron-scale objects however requires a well-balanced system design and sophisticated reconstruction algorithms, that are commercially available, however not accessible cost-efficiently. Here, we present an open-source implementation of a lens-less digital inline holographic microscope platform, based on off-the-shelf optical, electronic and mechanical components, costing less than \$190. It employs a Blu-Ray semiconductor-laser-pickup or a light-emitting-diode, a pinhole, a 3D-printed housing consisting of 3 parts and a single-board portable computer and camera with an open-source implementation of the Fresnel-Kirchhoff routine. We demonstrate 1.55 μm spatial resolution by laser-pickup and 3.91 μm by the light-emitting-diode source. The housing and mechanical components are 3D printed. Both printer and reconstruction software source codes are open. The light-weight microscope allows to image label-free micro-spheres of 6.5 μm diameter, human red-blood-cells of about 8 μm diameter as well as fast-growing plant *Nicotiana-tabacum*-BY-2 suspension cells with 50 μm sizes. The imaging capability is validated by imaging-contrast quantification involving a standardized test target. The presented 3D-printable portable open-source platform represents a fully-open design, low-cost modular and versatile imaging-solution for use in high- and low-resource areas of the world.

Introduction

Digital inline holography (DIHM) is an imaging modality within the fast evolving field of imaging microscopy research since a few decades [1] and is based on Gabor's holographic principle [2]. By wide-field illumination of semi-transparent nano- to micron-sized objects with either a coherent or incoherent point light source, an interference pattern forming the hologram is created within a detection plane. It consists of the scattered part of the beam, object beam, and the unscattered (transmitted) part, the reference beam. The hologram contains amplitude and phase information of the imaged objects and allows for a numerical reconstruction of the object's light field. To date, digital holography has been pioneered across a broad range of the electromagnetic spectrum: Terahertz[3] and infrared [4] holography bear the attractive potential to penetrate opaque media, whereas UV [5, 6] and X-ray [7, 8] illumination enable imaging on nanometer scale. Electron holography today is a mature research field and widely in use, allowing for molecular imaging [9, 10]. Digital holography within the visible wavelength regime has attracted considerable attention where a broad spectrum of light sources has been employed, ranging from gas [11, 12], solid state [13] and semiconductor [1, 14, 15, 16] lasers over light emitting diodes (LEDs) [17, 18, 19, 20] to halogen lamps [21]. Recently, ultra-broadband digital holography with sunlight illumination has been demonstrated, employing a new reconstruction algorithm [22]. In digital off-axis holography (DOAH), reference and object beam are spatially separated and recombine at an angle within the detector plane. Such experiment can already be compact, combining for example a collimation lens and two gradient-index lenses forming the point-light source and which enables a highly stable off-axis digital holographic system [23]. This helps reducing twin images, typically a challenge in holography set-ups [24]. During reconstruction a conjugate, out of focus image of the object is obtained in addition to the reconstructed object. This can lead to residual fringes, decreased contrast and an over all reduced image quality. In DOAH, object and twin image can be separated in the Fourier domain of the hologram. DOAH set-ups require a rather large number of optical components including mirrors, beam splitters and collimation lenses. Complementary to DOAH, DIHM constitutes a compact holography implementation

that avoids to spatially separate the reference beam from the object beam. DIHM setups typically comprise of coherent or incoherent point light source, a 2D digital detector array and, positioned in between, the micron-scale object sample to be imaged. It has been demonstrated in the ultraviolet[5], visible[13], near-infrared[25] up to the mid-infrared[26] wavelength regime. In DIHM, only a negligible influence of the twin image on the quality of microscopic object analysis has been demonstrated [1, 27], as the twin image is defocused across the whole detector array when the distance between detector and object is large as compared to the object size. Moreover, for DIHM several approaches to numerically remove the twin image from the reconstructed image have been demonstrated [28, 29, 30]. Ideal light sources are semiconductor photonic emitters such as laser diodes (LDs) and LEDs thanks to their compactness, high electro-optical efficiencies, comparable low price and availability. Partially coherent light sources can even enhance the result in DIHM as coherent speckle noise is reduced [27] while being less susceptible to mechanical vibrations. Considering the generally less complex implementation, easy replacement, lower price, high reliability and reduced safety issues, LEDs appear as ideal DIHM light sources for student and early researcher education. To ensure homogeneous illumination, the LED or LD light can be coupled into an optical fibre ensuring a Gaussian beam profile at the fibre’s end [19, 31, 20, 15, 32]. In addition, more compact or complex experimental set-ups can be realized thanks to the mechanical fibre flexibility [31]. Both charge-coupled device (CCD) and complementary metal-oxide-semiconductor (CMOS) cameras are commonly used as detectors, with an increasing number of CMOS chips due to recent advances in terms of sensitivity and reduced pixel size. Two parallel tracks of current DIHM research can be identified, focusing on two different detection schemes: On-chip microscopy on the one hand, where the sample under investigation is located close to the CMOS detector. Its advantage is the large field-of-view which corresponds to the whole detector area. Several on-chip microscopes employing low-coherent LED illumination [17, 31, 33] have been demonstrated making them already cost-efficient and easy to operate. In combination with several pixel super-resolution approaches using multi-height imaging [19], wavelength scanning [20], sub-pixel shifting[34] or flowing samples [35], sub-micron spatial resolution is possible. Sub cellular imaging of malaria infected blood cells [36], red blood cell (RBC) imaging with a cell phone camera [18] and colour imaging using DIHM [31] have been reported. On the other hand, fringe magnification technique is studied where the sample is located near the point source [1, 23, 15]. Here, the maximum lateral resolution δ_{lat} is accompanied by a decreased field-of-view (see equation (5)).

DIHM research has already reached the stage of commercialization where for example several DIHM implementations exist including lens-less inline and DOAH schemes [37] delivering lateral resolutions of $0.3\ \mu\text{m}$. A submersible holographic microscope for remote in-vivo oceanic microscopy has been reported [38] and is now commercially available [39]. Moreover, lens-based DOAH has recently been employed in in-line industrial production control [40] and for imaging of semiconductor structures [41]. In life-sciences, DIHM has the advantage of working label-free, which enables non-invasive, in-vivo study of biological samples, for example RBCs[42, 43, 44], parasited mouse RBCs [45], sperm cells [15], diarrhea parasites [17], and several aquatic organisms [38]. Moreover, as information about the whole sample volume is encoded in one single hologram, processing speed is substantially increased as compared to microscopic scanning techniques such as confocal or fluorescence microscopy. Thus, large sample volumes can be analyzed efficiently, such as cell cultures of human cancer cells [46, 47] as well as microplastic pollution in marine environments [48]. Furthermore, by acquiring and analyzing sequences of images, DIHM enables long term cell evolution studies [32] and micro-particle tracking [49]. Although differently complex, portable and low-cost DIHM solutions have recently been reported [50, 18, 15, 51], critically important details necessary for their realization in a laboratory are mostly disclosed. Such important details include details on employed of light sources, distances between objects and light source or detector, methods of reconstruction, non obvious limitations or design or construction files thus making it challenging to set up a DIHM without too much prior expertise and avoids access to low-cost micron spatial resolution imaging. In this work first, we present two experimental DIHM platforms employing an LED and a LD as illumination sources and operate the both by a portable single-board computer and camera. The LD has been disassembled from a standard commercially available Blu-ray disk drive. The housing and all mechanical mounts are 3D printed. [52]. Second, we describe the implemented open-source hologram reconstruction based on HoloPy [53] and Fiji plugin [54]. All employed code is open-source accessible aiming at triggering further developments and sharing between research laboratories, diagnostic labs and science education. Third, we demonstrate microscopic 2D-imaging of polystyrene micro-spheres (PMSs) and mature human RBCs imaging with micron spatial resolution. Fourths, we perform 2D-imaging of larger tobacco BY-2 cells (TBY2s). Fifths, we quantify the achieved spatial resolution by optical contrast analysis of an united states air force (USAF) microscopic imaging test target. Sixths, we summarize our

efforts in developing a 3D-printable open-source platform for cellular imaging and provide a brief outlook on our activities.

Laboratory and 3D printed opto-mechanical DIHM setups

Both developed DIHM implementations, described in the following, aim at achieving and validating the maximum achievable spatial resolution when an temporally and spatially coherent source as well as a temporally and spatially incoherent semiconductor light source at equivalent emission wavelength are considered. First, a LD-based lens-less DIHM platform is developed that aims at demonstrating single-digit micrometer spatial resolution cellular imaging by a temporally coherent source and is schematically depicted in Fig. 1 (a). It employs a 405 nm emitting LD in a laser-pickup which has been dismantled from a commercially available standard Blu-ray disc drive. The laser emission is coupled into a standard single-mode fibre. The diverging fundamental Gaussian mode beam is directed towards the object glass plate at a distance of 24.09 mm from the fibre exit facet. The CMOS camera is positioned at a distance of $f = 30$ mm. Second, an LED-based lens-less DIHM platform depicted schematically in Fig. 1 (c) is designed and constructed by 3D printable parts, with the over all system costs amounting to less than \$ 190. Compared to Fig. 1 (a), in Fig. 1 (b) a 430 nm emitting high-power LED is employed as a temporally and spatially incoherent semiconductor light source. A fraction of the emitted light is passed through a high-precision pinhole where 1.1 μ W of optical power are emitted at the pinhole for an injection current of 125 mA and impinge on objects to be imaged ($z = 5.91$ mm). For live cell imaging, such ultra-low optical power is of critical importance, as cell damage by light exposure needs to be minimised. To construct the LED-based platform in Fig. 1 (b), first three mechanical parts in Fig. 1 (c) are 3D-printed, see section “Methods”, and assembled as sketched in Fig. 1 (d) and e) where also specific dimensions of the platform are depicted. For both experiments, equal spatial separations between emission facet, microscope glass plate carrying the micro-objects under investigation and CMOS detector are chosen. We chose a distance of 30 mm between light source and detector in order to reach a compact experimental set-up, while still maintaining illumination of the hole detector area. The position of the object emerges from resolution optimization, see section “Resolution”. A Raspberry Pi single-board portable computer and a Raspberry Pi CMOS detector camera with a pixel size of $(1.12 \times 1.12) \mu\text{m}^2$ serve as light source current injection

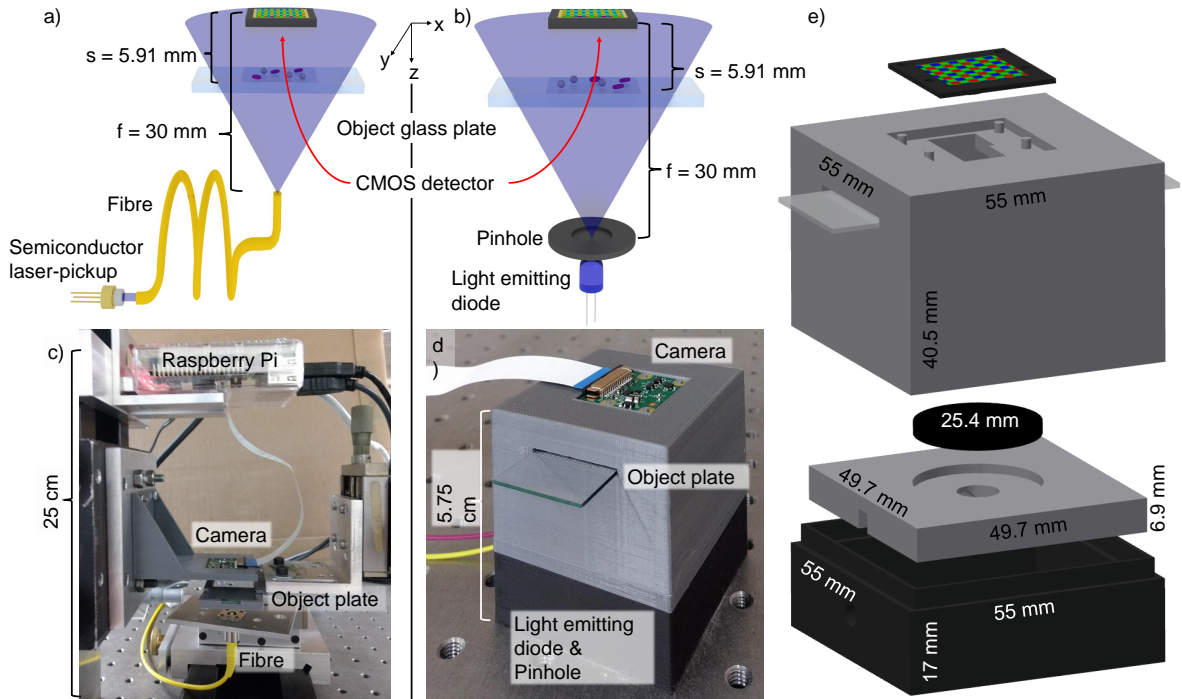


Figure 1: Developed laboratory DIHM and 3D printable DIHM setup. Schematics of the a) fibre-coupled LD pickup inline illumination. b) LED pinhole setup. c) Image of the laboratory fibre-coupled laser-pickup setup and dimensions. d) Image of the complete 3D-printed LED set-up. e) Exploded view of the three developed and used 3D printed parts with dimensions (CAD files open accessible, see methods chapter). Schematically depicted light propagation not to scale.

driver and hologram acquisition, see section “Methods”. A constant injection current of 28 mA for the LD were provided by a commercial LD driver, while a current of 125 mA for the LED was provided by a simple electrical circuit made of off the shelf components. A conventional rechargeable power bank battery pack provides electrical energy for the computer. Estimated theoretical spatial resolutions δ of $\delta_{\text{Laser}} = 0.87 \mu\text{m}$ and with an LED light source of $\delta_{\text{LED}} = 0.92 \mu\text{m}$ at an available CMOS pixel size of $1.12 \mu\text{m}$ and at a distance of $f = 30 \text{ mm}$ between fibre facet and CMOS detector are expected for the LD and LED light source, respectively.

Image reconstruction

Following the hologram acquisition, information retrieval of the cellular objects deposited on the object glass plate is performed numerically. The propagation of light fields is completely described by diffraction theory. Hence it is possible to reconstruct amplitude and phase information of the objects from their interference patterns generated on the camera. At the object location the pattern is focused and reveals the shape and morphology of micro-objects. Numerically, arbitrary planes can be re-focused in retrospect yielding access to volumes with a large number of objects in different heights in z-direction which can be studied with acquiring a single image. The propagation of a wave front towards the detector is described by the Fresnel-Kirchhoff diffraction integral

$$U_{\text{det}}(X, Y) = -\frac{i}{\lambda} \iint U_{\text{in}}(x, y) t(x, y) \frac{\exp\left(ik|\vec{r} - \vec{R}|\right)}{|\vec{r} - \vec{R}|} dx dy, \quad (1)$$

where $U_{\text{det}}(X, Y)$ denotes the wave field on the detector, $U_{\text{in}}(x, y)$ is the incident wave, $t(x, y)$ the transmission function of the object, and $\vec{r} = (x, y, z)$ and $\vec{R} = (X, Y, 0)$ are two points in the object plane respectively detector plane[55]. The amplitude and phase distribution of the object can be obtained via an inverse integral

$$U_{\text{obj}}(x, y) = \frac{i}{\lambda} \iint U_{\text{ref}}(X, Y) H_{\text{det}}(X, Y) \frac{\exp\left(-ik|\vec{r} - \vec{R}|\right)}{|\vec{r} - \vec{R}|} dX dY, \quad (2)$$

with the reference wave $U_{\text{ref}}(X, Y)$ and the intensity distribution of the hologram in the detector plane $H_{\text{det}}(X, Y)$. For the reconstruction, an open-source plugin for the open-source microscope software Fiji, see “Methods” section, that implements the angular spectrum estimation for small distances in the order of micrometers up to several centimeters, is employed. The amplitude distribution in the reconstructed plane is calculated using two Fourier transforms

$$U_{\text{obj}}(z) = \mathcal{F}^{-1} \left\{ \mathcal{F}\{U_{\text{det}}\} \exp\left(iz\sqrt{k^2 - \frac{4\pi^2 n^2}{Np}}\right) \right\}, \quad (3)$$

where z is the height of the reconstructed plane, k the wave vector, n the index of refraction, N the number of pixels and p the pixel size of the CMOS detector. \mathcal{F} and \mathcal{F}^{-1} denote Fourier Transform and the inverse Fourier Transform. The formalism described above is implemented in two open-source reconstruction software packages, see “Methods” section. In the following, we elaborate and identify two easy to implement reconstruction softwares on a standard desktop computer or potentially also on a mobile phone. HoloPy, a software package for python, allows for hologram reconstruction, but also hologram simulation and scattering calculations. The algorithm to reconstruct point source holograms is based on Fresnel-Kirchhoff diffraction[1]. It considers a background subtracted hologram, experimental parameters including distances and light source wavelengths and then reconstructs the hologram using two Fourier transforms. Alternatively, hologram fitting is provided by HoloPy where the position of a scatterer is simulated in order to produce the same interference pattern instead of image back-propagation [56]. For the case of a known number of scatterers, this method can be recommended as it allows to reconstruct spherical or cylindrical object shapes. It is less practicable, however, when arbitrarily shaped micro-objects are of interest, as for example folded RBCs. For the latter case, an open-source plugin [57] for Fiji, see “Methods” section, is a possible solution with a user-friendly graphical-user-interface, implemented in Java. Phase, amplitude and intensity distribution of micro-objects can be reconstructed at arbitrary heights in z-direction.

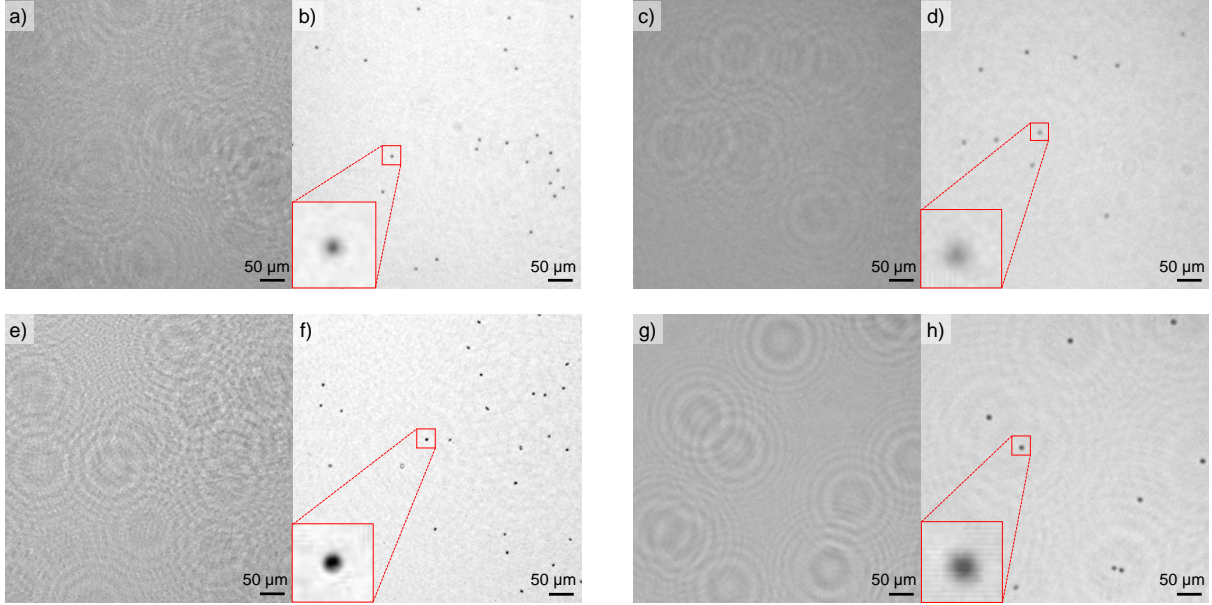


Figure 2: Holograms and according reconstructions of PMSs and human RBCs. Each inset shows a single sphere or RBC enlarged to five times its original size. a) Hologram of PMSs captured with LD setup. b) Reconstruction of (a). c) Hologram of PMSs captured with LED setup. d) Reconstruction of (c). e) Hologram of RBCs captured with laser setup. f) Reconstruction of (e). g) Hologram of RBCs captured with LED setup. h) Reconstruction of (g).

Micro particle and cellular imaging

In the following, we first capture and image standardized PMSs of diameter $(6.5 \pm 0.2) \mu\text{m}$ by both the LD and LED-based lens-less DIHM platform and reconstruct the resulting object properties by the Fiji plugin. Second, we investigate anonymized mature RBCs as micro-objects in the same manner. Third, we image cell suspension culture TBY2s. The recorded holograms and subsequently reconstructed object planes for multiple PMSs and RBCs are depicted in Fig. 2. Laser-based DIHM hologram (a) and reconstruction (b) is presented next to LED-based DIHM hologram (c) and reconstruction results (d). Both insets depict an isolated PMS or RBC enlarged to five times its original size. It becomes evident that the LD-based platform provides sharper images where a larger number of interference fringes can be captured per object. These fringes overlap within the hologram resulting in a hologram with more grainy texture as compared to the LED-based results in Fig. 2 (a,c). In contrast, the LED-based reconstructed image is considerably more washed out resulting in comparably extended objects. Accordingly, for human RBCs imaged by the LD-based platform, the oval disk shape can clearly be resolved as depicted in Fig. 2 (e,f). Several RBCs appear to be tilted in their spatial position, resulting in an elliptical shape. This is in stark contrast to the results obtained by the LED-based platform where information retrieval, for example on the cell morphology, are scarce. However, by the LED-based platform, individual cells can clearly be distinguished, thus exemplifying its potential for individual cell counting or tracking. In order to validate both platform's imaging capabilities also for extended cellular objects, fast growing plant tobacco TBY2s have been prepared and imaged. TBY2s are employed in various fields of plant biology as a model material and are ideally suited for cellular and molecular analyses[58]. Corresponding results are depicted in Fig. 3. The recorded holograms and reconstructed object planes for an isolated TBY2 are depicted for LD-based DIHM hologram (a) and reconstruction (b) is presented whereas the hologram, obtained by the LED-based DIHM, is depicted in (c) and the corresponding reconstruction in (d). Both platforms allow to successfully access individual cell segments with a length of $50 \mu\text{m}$ as well as internal structures including cell nuclei and vacuoles. In Fig. 3(b), a dividing cell undergoing mitosis can be observed. For LED illumination, individual vacuoles are not distinguishable. This is not surprising, as the vacuole membrane thickness is around one order of magnitude smaller than the cell wall thickness of $(7-10) \text{ nm}$ for plant vacuoles[59] as compared to $(71-87) \text{ nm}$ for tobacco leaf cells walls [60]. However it is possible to make out the nuclei of several cells. Interestingly, TBY2s infer a more complex interference pattern as compared to both PMSs and RBCs, indicating a stronger absorption and thus increased hologram contrast. We found that Fiji revealed a substantially faster reconstruction as compared to

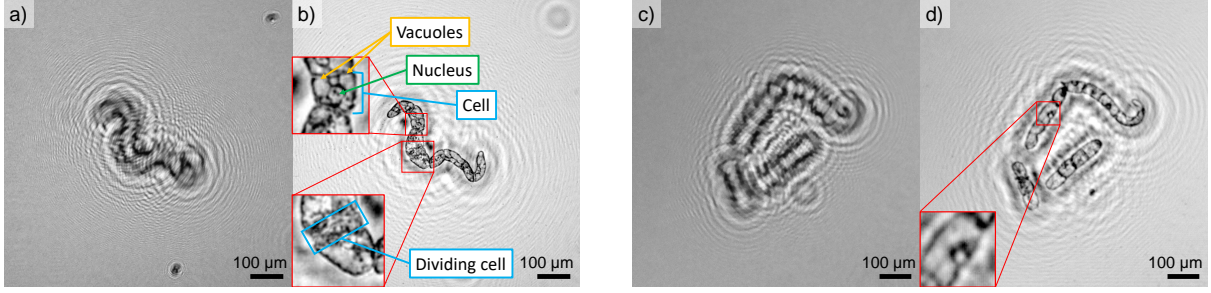


Figure 3: Holograms and according reconstructions of TBY2s. The insets are depicted magnified by a factor of three. a) Hologram captured with LD setup. b) Reconstruction of (a). c) Hologram captured with LED setup. d) Reconstruction of (c).

HoloPy. The reconstruction of 10 planes of a digital hologram by the Fiji plugin demands 30 seconds computational time on a regular consumer PC as compared to several minutes by HoloPy. Towards larger volumes, the reconstruction time can theoretically be improved by performing computations on a graphics processing unit [11] as demonstrated for live imaging [61]. In the following section, we aim to quantify the theoretical lateral resolution as well as the spatial resolution experimentally achieved by both the LD-based and LED-based DIHM platforms.

Resolution

In DIHM, the lateral resolution is bounded by the optical assembly numerical aperture (NA) and the illumination wavelength λ [1]:

$$\delta_{\text{lat}} = \frac{\lambda}{2NA}, \quad (4)$$

suggesting a shorter wavelength for a higher lateral resolution. For a digital holographic microscope with a pixel number N , with pixel size p , an illumination wavelength λ and a distance s between object and detector plane, this translates to

$$\delta_{\text{lat}} = \frac{s\lambda}{Np}. \quad (5)$$

As described in [62], a maximum lateral resolution can be achieved at a distance

$$s_{\text{opt}} = \frac{f}{1 + \frac{f\lambda}{Np^2}} \quad (6)$$

between object and detector, with the distance f between light source and detector. This originates from the consideration, that a higher resolution is possible, the closer the object is placed to the detector, however at the same time the interference fringes move closer. Here, s_{opt} denotes the distance at which different interference rings are still resolved by different camera pixels. The axial resolution of the system can be calculated according to

$$\delta_{\text{ax}} = \frac{\lambda}{2(NA)^2} = \frac{2s^2\lambda}{(Np)^2}. \quad (7)$$

By equation (6), the theoretical resolution for both developed platforms can be estimated. For $p = 1.12 \mu\text{m}$, $N = 2464$, $f = 30 \text{ mm}$, $\lambda_{\text{LED}} = 430 \text{ nm}$ and $\lambda_{\text{Laser}} = 405 \text{ nm}$, respectively, lateral resolutions of $\delta_{\text{LED}} = 0.92 \mu\text{m}$ and $\delta_{\text{Laser}} = 0.87 \mu\text{m}$ are theoretically possible by the selected, optimum platform design. To evaluate the experimentally achieved resolution, a 1951 USAF microscopic imaging test target on a glass microscopic slide serves as a reference object consisting of groups of horizontal and vertical lines with decreasing spatial frequency. The resulting reconstructed amplitude images acquired with the LED (a) and LD (b) setup are depicted in Fig. 4. With LED illumination, element 1 of group 7 is the last resolvable element corresponding to a resolution of 128 line pairs/mm and a line width of $3.91 \mu\text{m}$. For LD illumination, element 3 of group 8 is still resolvable, leading to a resolution of 322.5 line pairs/mm and a line width of $1.55 \mu\text{m}$. This is mostly a result of the higher temporal and spatial resolution of the laser in comparison to the used LED, as well as the smaller wavelength. The resolving power with LD illumination is thus significantly higher.

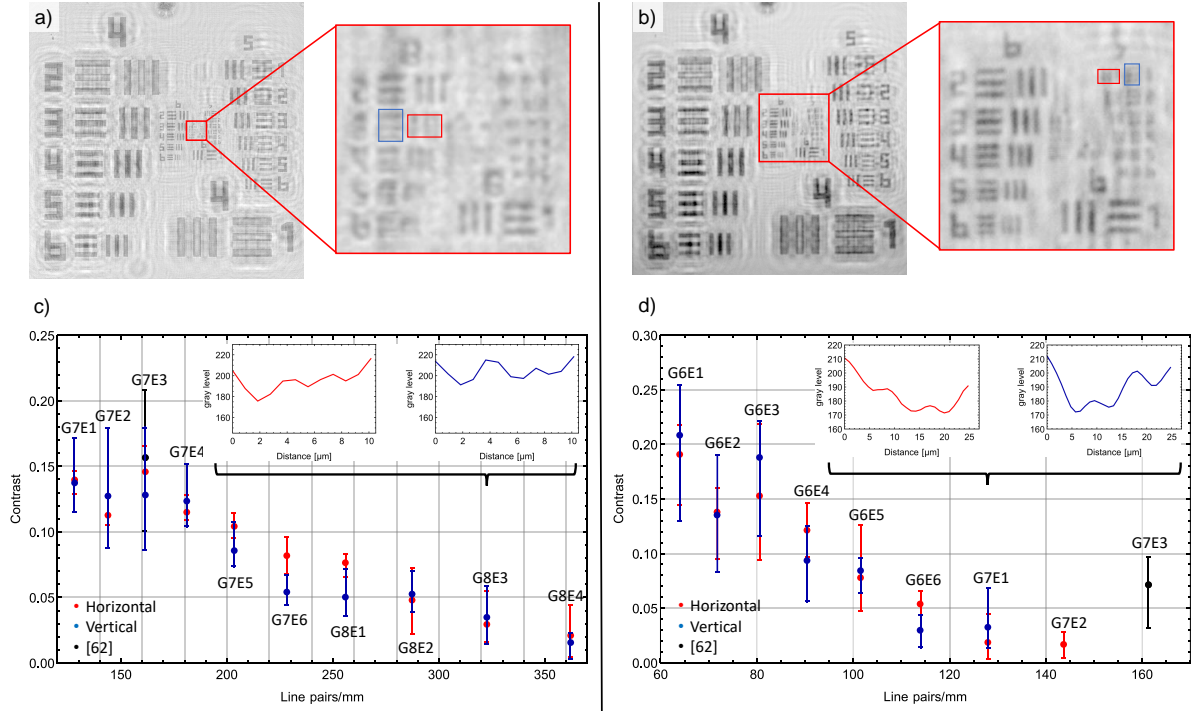


Figure 4: Imaging of a 1951 USAF target to quantify the accessible spatial resolution. a) LD setup. Groups 8 and 9 are shown enlarged. b) LED setup. Groups 6 to 9 are shown enlarged. c) Contrast of the different elements for LD illumination. The inset shows the intensity profile plot for horizontal and vertical elements 3 of group 8. d) Contrast for LED illumination. Additionally included are reported contrast values [63], where either an unspecified laser or an LED emitting at 470 nm (25 μm pinhole) had been employed (not specified further).

Finally, to quantify the achieved image contrast and thus evaluate the capability of the developed DIHM setups, in the following the intensity of a single USAF element is averaged along its axis and plotted (see red and blue rectangle in Fig. 4a and b). Then, the contrast of consecutive extreme points is calculated by $K = \frac{I_{\max} - I_{\min}}{I_{\max} + I_{\min}}$. Each element consists of 5 dark lines which leads to 4 contrast values. The average contrast is then displayed in dependence on the resolution in line pairs/mm, with the error bars ranging from the minimum to the maximum value. The resulting image contrast of different elements of the respective USAF image is depicted in Fig. 4c) and d). Results obtained by both light sources indicate decreasing contrast values with increasing line pairs. The maximum resolvable elements are as shown by the the intensity profile plots for horizontal and vertical elements 3 of group 8 in the inset of Fig. 4c). For LED, the maximum resolvable element is element 1 of group 7 as depicted in the inset of Fig. 4d). We compared our contrast values to reported values [63], where an unspecified laser or a LED with a central wavelength of 470 nm (25 μm pinhole) was used for image acquisition. The reported value for laser illumination coincides with our results. With LED illumination, the reported value reaches a higher resolution, group 7 element 3 is still resolvable. This could be due to a higher signal-to-noise ratio of the employed camera, the smaller bandwidth of only 10 nm as well as the use of advanced reconstruction algorithms. The achieved spatial resolution of both setups is suited to image and detect individual micro-particles and cellular objects including ensembles of microscopic biological samples. For the LD-based DIHM, sharper interference pattern and a higher number of interference fringes could be captured. Thus, more object information is retrieved yielding a crisper reconstructed image including more details. We attribute this to the LD's higher second-order temporal coherence as well as spatial coherence. The LED's spatial coherence could be increased by reducing the pinhole diameter which would require increased LED biasing currents which then require efficient cooling of the LED and thereby increasing the physical dimensions of the setup. Our DIHMs allow to image cellular objects with dimensions smaller than 10 μm as well as microscopy of larger objects with a spatial resolution of 3.91 μm. To ensure maximum possible resolution, a LD-based DIHMs is recommended, whereas for applications where high temporal stability, compact set-up, ruggedness and reduced costs a required, LED-based DIHMs is recommended.

Conclusion

A 3D printable platform for lens-less holographic cellular imaging with open accessible software solutions has been developed delivering spatial resolutions of $1.55\ \mu\text{m}$ by LD or $3.91\ \mu\text{m}$ by LED illumination. A 405 nm Blu-ray semiconductor laser-pickup coupled to an optical fibre and a 430 nm high power LED in combination with a $15\ \mu\text{m}$ pinhole have been successfully employed as DIHM light sources. Despite its lower degree of temporal coherence, the LED proved to be of advance in terms of implementation, price and lower safety concerns. A single-board portable Raspberry Pi computer and camera operate the light sources as well as perform the image acquisition. By an open-source software implementation of the Fresnel-Kirchhoff algorithm, we imaged and successfully reconstructed $6.5\ \mu\text{m}$ PMS and human RBCs with a diameter of about $8\ \mu\text{m}$, as well as TBY2s with an individual size of about $50\ \mu\text{m}$. Less than $1.1\ \mu\text{W}$ of optical power were sufficient for holographic imaging microscopy. Such ultra-low optical power can be of critical importance for live cell imaging where light exposure of the cells needs to be as low as possible. Equally compact setup could be envisioned for the LD when fibre-coupled LDs are available, which are however considerably expensive. The DIHM setup presented here may serve as a reliable, easy to implement and flexible to extend solution for student an early researcher education and for different demands in microscopic imaging. The total costs for the LED setup amount to \$190 (\$3 LED, \$75 Pinhole, \$35 Raspberry Pi 3, \$25 Raspberry Pi Cam v2, \$25 3D print, \$27 power bank) and thus enables a convenient entry into the wide field of digital holography. Future work could include the integration of the DIHM with micro-fluidic channels [49, 64, 65] or considering machine learning algorithms to automatically count and identify particles [66], as well as diagnose illnesses such as meningitis [67], iron-deficiency anemia or diabetes mellitus [68]. The developed 3D-printable photonic platform might help facilitating reproducibility of results obtained in different laboratories and prototyping of specific improvements and advancements of the DIHM setups. The cost-efficient open science and open hard and software platform aims in particular at contributing towards a democratization of scientific knowledge [69].

Methods

DIHM construction, light sources, opto-electronics, electrical circuits and 3D print

The Blu-ray LD-pickup (SF-AW210) has been dismantled from a commercially available standard computer Blu-ray optical head and its emits a maximum optical output power of 300 mW at a wavelength of 405 nm for an injection current of 150 mA. The LD-pickup beam is collimated and focussed by two aspheric lenses with an effective focal length of 11 mm (\$87 each, C220TMD-A, Thorlabs Inc.) into a 2 m long silica core FC/PC single-mode optical fibre with a core diameter of $3\ \mu\text{m}$ (\$99, S405-XP, Nufern Inc.) the coupling is adjusted to ensure a low laser power of $24.5\ \mu\text{W}$ at the fibre exit which proved optimum for DIHM imaging. The emitted divergent beam (Rayleigh length $z_r = 21\ \mu\text{m}$) has TEM₀₀ intensity profile and a mode field diameter of $2w_0 = 3.3\ \mu\text{m}$. Within the plane of the object glass plate, at $z = 5.91\ \text{mm}$, the divergent beam impinges the objects under investigation with a power density of $4.2\ \mu\text{Watt}/\text{mm}^2$ and with a beam diameter of $3.8\ \text{mm}$ ($1/e^2$). In the CMOS detector plane ($f = 30\ \text{mm}$), the beam diameter amounts to $4.7\ \text{mm}$ ($1/e^2$). The high-power LED (\$3, 3W High Power LED 430nm - 435nm hyper violet, Avonec, Germany [70]) emits at wavelengths centered at around 430 nm with spectral bandwidth of $\Delta\lambda_{\text{LED}}$ of 15 nm (full-width-half-maximum) corresponding to a coherence length of $L_{c,\text{LED}} = \lambda_{\text{LED}}^2 \times (\pi \times \Delta\lambda_{\text{LED}})^{-1} = 3.9\ \mu\text{m}$ for a Gaussian intensity distribution, with $\Delta\lambda$ the full width at half-maximum spectral line width [71]. A high-precision stainless steel pinhole with a diameter of $(15 \pm 1.5)\ \mu\text{m}$ (\$75, P15D, Thorlabs Inc.) has been employed as all 3D printing attempts yet did not yield a necessary sufficiently high mechanical grade circular diameter. All necessary parts for the LED setup can be found at <https://github.com/teph12/DIHM>. All parts and Raspberry Pi housing were printed with a commercial 3D-printer (\$880, Prusa i3 MK3, Prusa Research s.r.o.) using standard polylactide synthetic polymer filament with 1.75 mm diameter. A spatial printing resolution of 0.4 mm, parallel to the optical table, and 0.05 mm, in vertical or z-direction is available. Within the printed DIHM housing, LED and pinhole were fixed with tape (\$9, 3m-id 70005241826 Scotch Magic Tape, 3M Inc.). The case with VESA mounts for Raspberry Pi 3 (B/B+), Pi 2 B, and Pi 1 B+ can be accessed by [72]. The CMOS camera module is glued to the upper part of the box after removing the lens mounted in front of the module. We observed that otherwise strong hologram distortions appeared. In order to electrically bias the LD, a commercial LD driver was used to provide a constant output current. However, an

open-source driver is under construction while all parts are available for in total \$20[73]. For the LED, a custom soldered circuit has been developed accessing Raspberry Pi’s general purpose input/output (GPIO). The assembled system is depicted in 5b). The driver circuits can well be integrated into the 3D printed Raspberry Pi housing. A diagram of the circuit can be seen in Fig. 5a). The portable computer, camera and DIHM light sources are supplied with electrical power by a conventional power bank battery pack with maximum output power of 10 W (\$27, Aukey PB-N36). A computer monitor and computer mouse are required for the hologram acquisition. $V_BATTERY$ is the voltage provided by the power bank, whereas $V_TRIGGER$ is the voltage between the Raspberry Pi GPIO and ground. It triggers a transistor (BD135), which lets a current of 125 mA flow through the LED.

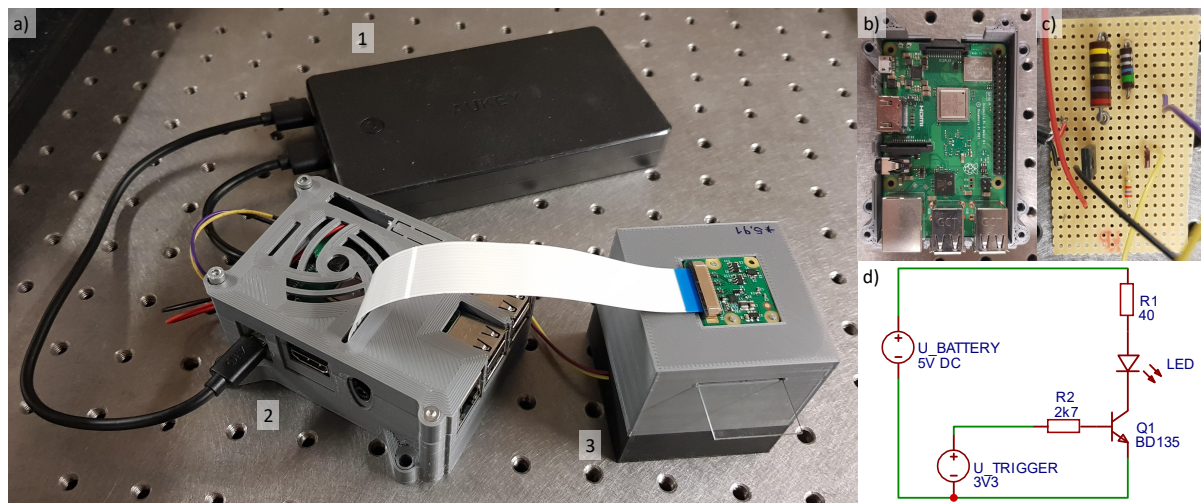


Figure 5: a) The fully portable DIHM system consisting of 1. USB-port power bank, 2. 3D printed housing containing Raspberry Pi and LED control circuit, 3. LED DIHM system as presented in Fig. 1d). b) Closeup of the Raspberry Pi single-board computer. c) Closeup of the LED control circuit. d) Schematic of the circuit for biasing the LED using the Raspberry Pi’s GPIOs.

Light source biasing, image detection and acquisition

A portable single-board computer and camera module with a 3280 x 2464 pixel CMOS chip and pixel dimensions of $(1.12 \times 1.12) \mu\text{m}^2$, sensor size $(3.674 \times 2.760) \text{mm}^2$ (\$35, Raspberry Pi 3 with \$25 Raspberry Pi Camera v2, Raspberry Pi Foundation, UK [52]) serve as light source driver and hologram acquisition.

Sample preparation

The RBC samples under investigation are standard anonymized RBC reference cells (\$27, A1A2B0 4x10, Immucor Med. Diagnostik GmbH, Germany). They are diluted in saline solution to a high degree (up to 0.02%). The employed polystyrene micro-spheres (\$129, BS-Partikel GmbH, Germany) have a diameter of $(6.5 \pm 0.2) \mu\text{m}$. They are equally high diluted in distilled water. Furthermore a few ml of ordinary dish detergent are added to prevent agglomeration and adhesion of the micro-spheres. After diluting the particular object a drop of the solution is placed by a standard plastic pasteur pipette on a high transmission flat glass microscope slide (75 mm x 25 mm x 1 mm, B270 I, SCHOTT AG) and then covered with a glass cover plate (22 mm x 22 mm x 0.15 mm, B270 I, SCHOTT AG)). *Nicotiana tabacum* cv. BY-2 suspension plant cell cultures[74] were grown in liquid saline medium based on a modified Linsmaier and Skoog medium with agitation on an incubator shaker. The cells have been grown in 50 ml medium within a 250 ml glass flask. Every 7 days, 5% inoculum had been transferred into a fresh medium [75, 76] and stored permanently on an incubator shaker.

Image acquisition, reconstruction and resolution validation

The pictures are acquired with a fixed white balance. For details see the camera file on <https://github.com/teph12/DIHM>. The image is then transferred to a PC with Windows 10 operating system and equipped with an Intel i3 processor and 8 GB of RAM, with Fiji installed. In Fiji the image is

converted to a 32-bit black and white picture, which is then loaded in the “Numerical Reconstruction” plugin. Here, using the parameters of image acquisition (distance between camera and object, wavelength, image size) the image is reconstructed. Subsequently the image contrast is normalized and enhanced by 0.2%. For the quantification of the experimentally achieved spatial resolution, a commercially available standardized 1951 USAF positive high-contrast chrome on quartz glass microscopic imaging test target created by photo lithography on a glass microscopic slide serves as a reference object (\$900, Ready Optics, US). It consists of groups of horizontal and vertical lines with standardized spatial frequencies starting at group 4, element 1 with 31 μm spacing and ending at group 11, element 6 with 137 nm spacing.

References

- [1] Manfred H. Jericho and H. Jürgen Kreuzer. Point source digital in-line holographic microscopy. In *Coherent Light Microscopy*, pages 3–30. Springer Berlin Heidelberg, 2010.
- [2] Dennis Gabor. A new microscopic principle. *Nature*, 161(4098):777–778, 1948.
- [3] Lu Rong, Tatiana Latychevskaia, Chunhai Chen, Dayong Wang, Zhengping Yu, Xun Zhou, Zeyu Li, Haochong Huang, Yunxin Wang, and Zhou Zhou. Terahertz in-line digital holography of human hepatocellular carcinoma tissue. *Scientific Reports*, 5(1), feb 2015.
- [4] L. Repetto, R. Chittofrati, E. Piano, and C. Pontiggia. Infrared lensless holographic microscope with a vidicon camera for inspection of metallic evaporations on silicon wafers. *Optics Communications*, 251(1-3):44–50, jul 2005.
- [5] Ahmad Faridian, David Hopp, Giancarlo Pedrini, Ulrike Eigenthaler, Michael Hirscher, and Wolfgang Osten. Nanoscale imaging using deep ultraviolet digital holographic microscopy. *Optics Express*, 18(13):14159, jun 2010.
- [6] Mustafa Ugur Daloglu, Aniruddha Ray, Zoltan Gorocs, Matthew Xiong, Ravinder Malik, Gal Bitan, Euan McLeod, and Aydogan Ozcan. Computational on-chip imaging of nanoparticles and biomolecules using ultraviolet light. *Scientific Reports*, 7(1), mar 2017.
- [7] Martin Krenkel, Mareike Toepperwien, Frauke Alves, and Tim Salditt. Three-dimensional single-cell imaging with x-ray waveguides in the holographic regime. *Acta Crystallographica Section A Foundations and Advances*, 73(4):282–292, 2017.
- [8] Tais Gorkhover, Anatoli Ulmer, Ken Ferguson, Max Bucher, Filipe R. N. C. Maia, Johan Bielecki, Tomas Ekeberg, Max F. Hantke, Benedikt J. Daurer, Carl Nettelblad, Jakob Andreasson, Anton Barty, Petr Bruza, Sebastian Carron, Dirk Hasse, Jacek Krzywinski, Daniel S. D. Larsson, Andrew Morgan, Kerstin Mühlig, Maria Müller, Kenta Okamoto, Alberto Pietrini, Daniela Rupp, Mario Sauppe, Gijs van der Schot, Marvin Seibert, Jonas A. Sellberg, Martin Svenda, Michelle Swiggers, Nicusor Timneanu, Daniel Westphal, Garth Williams, Alessandro Zani, Henry N. Chapman, Gyula Faigel, Thomas Möller, Janos Hajdu, and Christoph Bostedt. Femtosecond x-ray fourier holography imaging of free-flying nanoparticles. *Nature Photonics*, 12(3):150–153, 2018.
- [9] H.J. Kreuzer. Low energy electron point source microscopy. *Micron*, 26(6):503–509, 1995.
- [10] Hannes Lichte and Michael Lehmann. Electron holography—basics and applications. *Reports on Progress in Physics*, 71(1):016102, 2007.
- [11] P R Hobson, J J Nebrensky, and I D Reid. Challenges in using GPUs for the real-time reconstruction of digital hologram images. *Journal of Physics: Conference Series*, 415:012042, 2013.
- [12] Mehdi Molaei and Jian Sheng. Imaging bacterial 3D motion using digital in-line holographic microscopy and correlation-based de-noising algorithm. *Optics Express*, 22(26):32119, 2014.
- [13] Daniel Carl, Björn Kemper, Günther Wernicke, and Gert von Bally. Parameter-optimized digital holographic microscope for high-resolution living-cell analysis. *Applied Optics*, 43(36):6536, 2004.
- [14] Camila B. Giuliano, Rongjing Zhang, and Laurence G. Wilson. Digital inline holographic microscopy (DIHM) of weakly-scattering subjects. *Journal of Visualized Experiments*, (84), 2014.

- [15] Martín Sanz, José Ángel Picazo-Bueno, Luis Granero, Javier García, and Vicente Micó. Compact, cost-effective and field-portable microscope prototype based on MISHELF microscopy. *Scientific Reports*, 7:43291, 2017.
- [16] Manon Rostykus and Christophe Moser. Compact lensless off-axis transmission digital holographic microscope. *Optics Express*, 25(14):16652, 2017.
- [17] Onur Mudanyali, Cetin Oztoprak, Derek Tseng, Anthony Erlinger, and Aydogan Ozcan. Detection of waterborne parasites using field-portable and cost-effective lensfree microscopy. *Lab on a Chip*, 10(18):2419, 2010.
- [18] Derek Tseng, Onur Mudanyali, Cetin Oztoprak, Serhan O. Isikman, Ikbal Sencan, Oguzhan Yaglidere, and Aydogan Ozcan. Lensfree microscopy on a cellphone. *Lab on a Chip*, 10(14):1787, 2010.
- [19] Alon Greenbaum and Aydogan Ozcan. Maskless imaging of dense samples using pixel super-resolution based multi-height lensfree on-chip microscopy. *Optics Express*, 20(3):3129, 2012.
- [20] Wei Luo, Yibo Zhang, Alborz Feizi, Zoltán Göröcs, and Aydogan Ozcan. Pixel super-resolution using wavelength scanning. *Light: Science & Applications*, 5(4):e16060–e16060, 2015.
- [21] Stijn Vandewiele, Filip Strubbe, Caspar Schreuer, Kristiaan Neyts, and Filip Beunis. Low coherence digital holography microscopy based on the Lorenz-Mie scattering model. *Optics Express*, 25(21):25853, 2017.
- [22] Shaodong Feng and Jigang Wu. Differential holographic reconstruction for lensless in-line holographic microscope with ultra-broadband light source illumination. *Optics Communications*, 430:9–13, jan 2019.
- [23] Eugene Serabyn, Kurt Liewer, Chris Lindensmith, Kent Wallace, and Jay Nadeau. Compact, lensless digital holographic microscope for remote microbiology. *Optics Express*, 24(25):28540, 2016.
- [24] Emmett N. Leith and Juris Upatnieks. Reconstructed wavefronts and communication theory. *Journal of the Optical Society of America*, 52(10):1123, 1962.
- [25] Patrik Langehanenberg, Gert von Bally, and Björn Kemper. Application of partially coherent light in live cell imaging with digital holographic microscopy. *Journal of Modern Optics*, 57(9):709–717, may 2010.
- [26] M. Ravaro, M. Locatelli, E. Pugliese, I. Di Leo, M. Siciliani de Cumis, F. D’Amato, P. Poggi, L. Consolino, R. Meucci, P. Ferraro, and P. De Natale. Mid-infrared digital holography and holographic interferometry with a tunable quantum cascade laser. *Optics Letters*, 39(16):4843, 2014.
- [27] Myung K. Kim. Principles and techniques of digital holographic microscopy. *Journal of Photonics for Energy*, page 018005, 2010.
- [28] Tatiana Latychevskaia and Hans-Werner Fink. Solution to the twin image problem in holography. *Physical Review Letters*, 98(23), 2007.
- [29] Bing Kuan Chen, Tai-Yu Chen, Shau Gang Hung, Sheng-Lung Huang, and Jiunn-Yuan Lin. Twin image removal in digital in-line holography based on iterative inter-projections. *Journal of Optics*, 18(6):065602, 2016.
- [30] L Denis, C Fournier, T Fournel, and C Ducottet. Numerical suppression of the twin image in in-line holography of a volume of micro-objects. *Measurement Science and Technology*, 19(7):074004, 2008.
- [31] Alon Greenbaum, Alborz Feizi, Najva Akbari, and Aydogan Ozcan. Wide-field computational color imaging using pixel super-resolved on-chip microscopy. *Optics Express*, 21(10):12469, 2013.
- [32] Zak Frentz, Seppe Kuehn, Doeke Hekstra, and Stanislas Leibler. Microbial population dynamics by digital in-line holographic microscopy. *Review of Scientific Instruments*, 81(8):084301, 2010.
- [33] Gregor Scholz, Qifeng Xu, Torben Schulze, Heidi Boht, Kai Mattern, Jana Hartmann, Andreas Dietzel, Stephan Scherneck, Ingo Rustenbeck, Joan Daniel Prades, Sönke Fündling, Hutomo Suryo Wasisto, and Andreas Waag. Led-based tomographic imaging for live-cell monitoring of pancreatic islets in microfluidic channels. *Proceedings*, 1(4), 2017.

- [34] Waheb Bishara, Ting-Wei Su, Ahmet F. Coskun, and Aydogan Ozcan. Lensfree on-chip microscopy over a wide field-of-view using pixel super-resolution. *Optics Express*, 18(11):11181, 2010.
- [35] Waheb Bishara, Hongying Zhu, and Aydogan Ozcan. Holographic opto-fluidic microscopy. *Optics Express*, 18(26):27499, 2010.
- [36] Hongying Zhu, Serhan O. Isikman, Onur Mudanyali, Alon Greenbaum, and Aydogan Ozcan. Optical imaging techniques for point-of-care diagnostics. *Lab Chip*, 13(1):51–67, 2013.
- [37] LyncéeTec. Digital holographic microscopes. <https://www.lynceetec.com/>, 2019.
- [38] S. K. Jericho, J. Garcia-Sucerquia, Wenbo Xu, M. H. Jericho, and H. J. Kreuzer. Submersible digital in-line holographic microscope. *Review of Scientific Instruments*, 77(4):043706, 2006.
- [39] 4-Deep. Holographic & fluorescence microscopes. <http://4-deep.com/>, 2019.
- [40] Fraunhofer IPM. HoloTop - High-precision inline 3D measurement. <https://www.ipm.fraunhofer.de/en/bu/production-control-inline-measurement-techniques/applications/holotop-holographic-3d-object-measurement.html>, 2019.
- [41] Markus Finkeldey, Lena Göring, Carsten Brenner, Martin Hofmann, and Nils C. Gerhardt. Depth-filtering in common-path digital holographic microscopy. *Optics Express*, 25(16):19398, aug 2017.
- [42] Jun Hong Park, Taesik Go, and Sang Joon Lee. Label-free sensing and classification of old stored blood. *Annals of Biomedical Engineering*, 45(11):2563–2573, 2017.
- [43] Benjamin Rappaz, Alexander Barbul, Annick Hoffmann, Daniel Boss, Rafi Korenstein, Christian Depeursinge, Pierre J. Magistretti, and Pierre Marquet. Spatial analysis of erythrocyte membrane fluctuations by digital holographic microscopy. *Blood Cells, Molecules, and Diseases*, 42(3):228–232, 2009.
- [44] Johan Zakrisson, Staffan Schedin, and Magnus Andersson. Cell shape identification using digital holographic microscopy. *Applied Optics*, 54(24):7442, aug 2015.
- [45] HyunJoo Park, Sung-Hee Hong, Kyoohyun Kim, Shin-Hyeong Cho, Won-Ja Lee, Youngchan Kim, Sang-Eun Lee, and YongKeun Park. Characterizations of individual mouse red blood cells parasitized by babesia microti using 3-D holographic microscopy. *Scientific Reports*, 5(1), 2015.
- [46] Lena Kastl, Michael Isbach, Dieter Dirksen, Jürgen Schneckeburger, and Björn Kemper. Quantitative phase imaging for cell culture quality control. *Cytometry Part A*, 91(5):470–481, mar 2017.
- [47] Zahra El-Schich, Anna Leida Mölder, and Anette Gjørloff Wingren. Quantitative phase imaging for label-free analysis of cancer cells—focus on digital holographic microscopy. *Applied Sciences*, 8(7):1027, jun 2018.
- [48] F. Merola, P. Memmolo, V. Bianco, M. Paturzo, M. G. Mazzocchi, and P. Ferraro. Searching and identifying microplastics in marine environment by digital holography. *The European Physical Journal Plus*, 133(9), sep 2018.
- [49] Yong-Seok Choi and Sang-Joon Lee. Three-dimensional volumetric measurement of red blood cell motion using digital holographic microscopy. *Applied Optics*, 48(16):2983, 2009.
- [50] Thomas G. Dimiduk, Ekaterina A. Kosheleva, David Kaz, Ryan McGorty, Emily J. Gardel, and Vinothan N. Manoharan. A simple, inexpensive holographic microscope. In *Biomedical Optics and 3-D Imaging*. OSA, 2010.
- [51] Tomoyoshi Shimobaba, Yusuke Taniguchi, Atsushi Shiraki, Nobuyuki Masuda, and Tomoyoshi Ito. Portable and low-cost digital holographic microscopy using web camera, point light source LED and open-source libraries. In *Biomedical Optics and 3-D Imaging*. OSA, 2012.
- [52] Raspberry Pi Foundation. Raspberry pi - teach, learn, and make with raspberry pi. <https://www.raspberrypi.org/>, 2019.
- [53] Manoharan Lab, Harvard University. HoloPy: Holography and Light Scattering in Python. <https://holopy.readthedocs.io/en/3.1.1/index.html>, 2016.

- [54] Johannes Schindelin, Ignacio Arganda-Carreras, Erwin Frise, Verena Kaynig, Mark Longair, Tobias Pietzsch, Stephan Preibisch, Curtis Rueden, Stephan Saalfeld, Benjamin Schmid, Jean-Yves Tinevez, Daniel James White, Volker Hartenstein, Kevin Eliceiri, Pavel Tomancak, and Albert Cardona. Fiji: an open-source platform for biological-image analysis. *Nature Methods*, 9(7):676–682, jul 2012.
- [55] Tatiana Latychevskaia and Hans-Werner Fink. Practical algorithms for simulation and reconstruction of digital in-line holograms. *Applied Optics*, 54(9):2424, 2015.
- [56] Thomas G. Dimiduk, Rebecca W. Perry, Jerome Fung, and Vinothan N. Manoharan. Random-subset fitting of digital holograms for fast three-dimensional particle tracking [invited]. *Applied Optics*, 53(27):G177, aug 2014.
- [57] J Garcia-Sucerquia. Multispectral digital lensless holographic microscopy: from femtosecond laser to white light LED. *Journal of Physics: Conference Series*, 605:012011, 2015.
- [58] Ryusuke Yokoyama, Daisuke Tanaka, Takeshi Fujino, Takao Itoh, and Kazuhiko Nishitani. Cell wall dynamics in tobacco BY-2 cells. In *Tobacco BY-2 Cells*, pages 217–230. Springer Berlin Heidelberg, 2004.
- [59] K. Esau and V. I. Cheadle. An evaluation of studies on ultrastructure of tonoplast in sieve elements. *Proceedings of the National Academy of Sciences*, 48(1):1–8, jan 1962.
- [60] S. Hoffmann-Benning, L. Willmitzer, and J. Fisahn. Analysis of growth, composition and thickness of the cell walls of transgenic tobacco plants expressing a yeast-derived invertase. *Protoplasma*, 200(3-4):146–153, sep 1997.
- [61] Massimiliano Locatelli, Marco Ravaro, Saverio Bartalini, Luigi Consolino, Miriam S. Vitiello, Riccardo Cicchi, Francesco Pavone, and Paolo De Natale. Real-time terahertz digital holography with a quantum cascade laser. *Scientific Reports*, 5(1), aug 2015.
- [62] E. Serabyn, K. Liewer, and J. K. Wallace. Resolution optimization of an off-axis lensless digital holographic microscope. *Applied Optics*, 57(1):A172, 2017.
- [63] Shaodong Feng and Jigang Wu. Resolution enhancement method for lensless in-line holographic microscope with spatially-extended light source. *Optics Express*, 25(20):24735, 2017.
- [64] Fook Chiong Cheong, Priya Kasimbeg, David B. Ruffner, Ei Hnin Hlaing, Jaroslaw M. Blusewicz, Laura A. Philips, and David G. Grier. Holographic characterization of colloidal particles in turbid media. *Applied Physics Letters*, 111(15):153702, 2017.
- [65] Vittorio Bianco, Biagio Mandracchia, Valentina Marchesano, Vito Pagliarulo, Federico Olivieri, Sara Coppola, Melania Paturzo, and Pietro Ferraro. Endowing a plain fluidic chip with micro-optics: a holographic microscope slide. *Light: Science & Applications*, 6(9):e17055, 2017.
- [66] Mohendra Roy, Geonsoo Jin, Dongmin Seo, Myung-Hyun Nam, and Sungkyu Seo. A simple and low-cost device performing blood cell counting based on lens-free shadow imaging technique. *Sensors and Actuators B: Chemical*, 201:321–328, oct 2014.
- [67] Robin Delacroix, Sophie Nhu An Morel, Lionel Hervé, Thomas Bordy, Jean-Marc Dinten, Michel Drancourt, and Cédric Allier. Cerebrospinal fluid lens-free microscopy: a new tool for the laboratory diagnosis of meningitis. *Scientific Reports*, 7(1), jan 2017.
- [68] Geon Kim, YoungJu Jo, Hyungjoo Cho, Hyun seok Min, and YongKeun Park. Learning-based screening of hematologic disorders using quantitative phase imaging of individual red blood cells. *Biosensors and Bioelectronics*, 123:69–76, jan 2019.
- [69] Tom Baden, Andre Maia Chagas, Greg Gage, Timothy Marzullo, Lucia L. Prieto-Godino, and Thomas Euler. Open labware: 3-D printing your own lab equipment. *PLOS Biology*, 13(3):e1002086, mar 2015.
- [70] Avonec. <https://avonec.de/>, 2018.
- [71] Emil Wolf Leonard Mandel. *Optical Coherence and Quantum Optics*. Cambridge University Press, 1995.

- [72] 0110-M-P0. Raspberry Pi 3 (B/B+), Pi 2 B, and Pi 1 B+ case with VESA mounts. <https://www.thingiverse.com/thing:922740>, 2015.
- [73] Innolasers. <https://innolasers.com/>, 2013.
- [74] Toshiyuki Nagata, Yasuyuki Nemoto, and Seiichiro Hasezawa. Tobacco BY-2 cell line as the “HeLa” cell in the cell biology of higher plants. In *International Review of Cytology*, pages 1–30. Elsevier, 1992.
- [75] Eva Nocarova and Lukas Fischer. Cloning of transgenic tobacco by-2 cells; an efficient method to analyse and reduce high natural heterogeneity of transgene expression. *BMC Plant Biology*, 9(1):44, Apr 2009.
- [76] S. Mercx, J. Tollet, B. Magy, C. Navarre, and M. Boutry. Gene inactivation by crispr-cas9 in nicotiana tabacum by-2 suspension cells. *Frontiers in Plant Science*, 7:40, 2016.